



HAL
open science

A multi-isotopic study of the groundwaters from the Lower Triassic Sandstones aquifer of northeastern France: Groundwater origin, mixing and flowing velocity

Christophe Innocent, Wolfram Kloppmann, Romain Millot, Laurent Vaute

► To cite this version:

Christophe Innocent, Wolfram Kloppmann, Romain Millot, Laurent Vaute. A multi-isotopic study of the groundwaters from the Lower Triassic Sandstones aquifer of northeastern France: Groundwater origin, mixing and flowing velocity. *Applied Geochemistry*, 2021, 131, pp.105012. 10.1016/j.apgeochem.2021.105012 . hal-03745495

HAL Id: hal-03745495

<https://brgm.hal.science/hal-03745495>

Submitted on 13 Jun 2023

HAL is a multi-disciplinary open access archive for the deposit and dissemination of scientific research documents, whether they are published or not. The documents may come from teaching and research institutions in France or abroad, or from public or private research centers.

L'archive ouverte pluridisciplinaire **HAL**, est destinée au dépôt et à la diffusion de documents scientifiques de niveau recherche, publiés ou non, émanant des établissements d'enseignement et de recherche français ou étrangers, des laboratoires publics ou privés.



Distributed under a Creative Commons Attribution - NonCommercial 4.0 International License

1 **A multi-isotopic study of the groundwaters from the Lower Triassic Sandstones**
2 **aquifer of northeastern France : groundwater origin, mixing and flowing velocity.**

3

4 **Christophe Innocent, Wolfram Kloppmann, Romain Millot, Laurent Vaute.**

5

6 **Abstract**

7 Water samples from the Lower Triassic Sandstones aquifer (LTS), plus two waters from the
8 overlying Muschelkalk aquifer and one water from the Dogger limestones are the matter of this
9 geochemical and multi-isotopic study ($\delta^{18}\text{O}$, δD , $\delta^{34}\text{S}$, $^{87}\text{Sr}/^{86}\text{Sr}$, $\delta^{11}\text{B}$, $\delta^7\text{Li}$). In addition, C
10 isotopic compositions and ^{14}C activities were measured. This study aimed at constraining the
11 origin of waters, water/rock interaction processes, and groundwater flow and residence times
12 within their aquifer.

13 LTS groundwaters have a meteoric origin, some of them recording the very minor contribution of
14 Triassic brines from the deepest aquifer of the Paris Basin, especially at the west end of the
15 LTS aquifer. The two waters from the Muschelkalk aquifer (one of them being the famous Great
16 Source[®] of Contrexéville), as well as the Dogger water also originate ultimately from meteoric
17 waters.

18 Boron isotopes emphasize in some waters, especially South of the Bray-Vittel Fault (BVF),
19 interaction processes between fluids and clayey lithologies that are present in some places in
20 the aquifer, apart from the aquicludes. Sr and Li isotopic signatures measured in some LTS
21 waters, especially in the Vittel area South of the fault indicate that leakage processes probably
22 occur between the Muschelkalk aquifer and the LTS aquifer.

23 Calculated ^{14}C residence times indicate flowing velocities in the order of 1 to 3 meters/year,
24 depending on leakage rates. Velocities are found to decrease northwestwards, towards the
25 center of the Paris Basin. Geochemical differences between waters sampled North and South of
26 the BVF indicate that this major fault constrains the circulation of groundwaters in this area.

27
28
29
30
31
32
33
34
35
36
37
38
39
40
41
42
43
44
45
46
47
48

49 **Keywords**

50 Groundwaters of eastern France, Lower Triassic Sandstone aquifer, mineral waters, isotopes,
51 groundwater residence time, hydrochemistry

52 **1 - Introduction**

53 The management of water resource today is a major concern for sustainable growth in a context
54 of rapid climate change. Hence, it is important to better understand the origin and characteristics
55 of groundwaters. The quantitative assessment and management of water resource implies that
56 the timing of aquifer recharge and thus the residence time of groundwater within an aquifer has
57 to be constrained as precisely as possible. Several isotopic tools are used for this purpose,
58 such as ^3H for "young" groundwaters (a few tens of years) (e.g.; Fritz et al., 1991) or ^{36}Cl in the
59 case of very old, >100 ky, waters (e.g.; Guendouz and Michelot, 2006). However, ^{14}C is the
60 most commonly used isotope for groundwaters "dating". It allows to constrain residence times of
61 100- to 30,000 y-old groundwaters (e.g.; Wigley, 1975; 1976: Mook, 1980).

62 The qualitative assessment of groundwater resource is also a key problem. First, human
63 activities may directly trigger chemical pollution, like for example nitrates due to the utilization of
64 fertilizers. In addition, excess pumping of water resource may disturb the natural functioning of
65 an aquifer, changing groundwater circulation, enhancing in some cases the interconnexion of
66 different aquifers, resulting from leakage processes. It is thus very important to constrain the
67 geochemical characteristics of vulnerable groundwaters.

68 In this paper, we investigate the geochemical and isotopic characteristics of groundwaters of the
69 Lower Triassic Sandstones (LTS) aquifer from eastern France, in order to constrain the origin
70 and the circulation of groundwaters in their aquifer. In the northern part of the LTS aquifer,
71 groundwaters have been pumped continuously for more than one century until 2006, in order to
72 allow coal extraction from carboniferous deposits of northeastern France and southwestern
73 Germany. At present, the LTS aquifer is clearly overexploited, and its management is very
74 critical. First, it is the most important resource for drinking water in the area. In addition, LTS
75 waters are extensively used for industrial purpose, namely for bottled waters of groundwaters
76 coming from the overlying Muschelkalk aquifer, such as worldwide famous Vittel[®], Contrex[®],
77 Hépar[®] mineral waters. Thus it is very important to constraint the natural geochemical fingerprint

78 of LTS groundwaters, as well as the characteristics of water circulation, for a sustainable
79 management of this aquifer.

80 For this purpose, O and H isotopes of the water molecule, S and O isotopes of the dissolved
81 sulfates, Sr, B and Li isotopes were measured in groundwaters. In addition, ^{14}C activities and C
82 stable isotopes were measured in order to estimate the residence time of groundwater in their
83 aquifer.

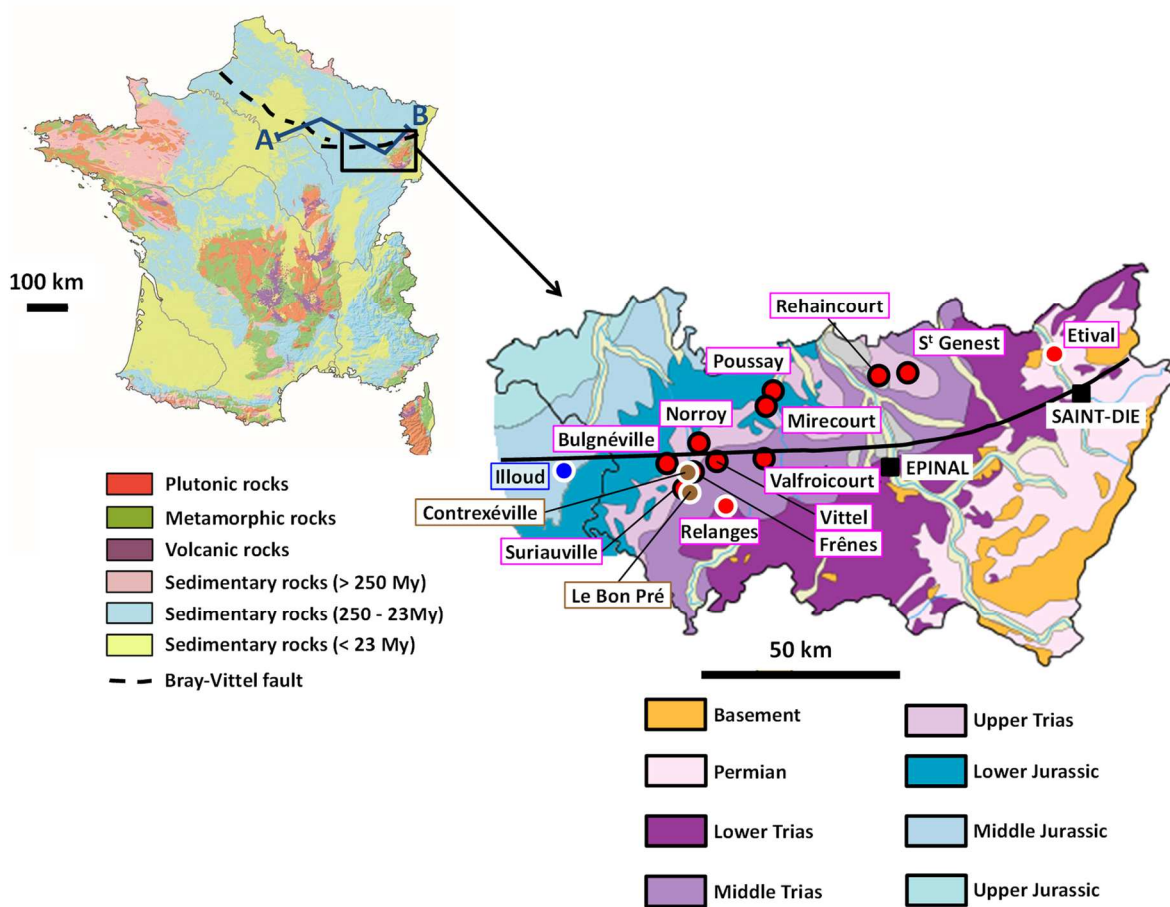
84

85 **2 - Geological and hydrogeological background**

86 The study area is located at the eastern edge of the Paris Basin (Fig. 1). The occurrence of
87 lower Triassic sandstones (Buntsandstein) is limited to the eastern part of the Paris Basin (Fig.
88 2). They are overlain by the Muschelkalk series, made of clays and limestones (Fig. 2). The
89 overlying Keuper series are characterized by evaporitic deposits in the eastern Paris Basin,
90 whereas they are mostly made of sandstones towards the centre of the basin (Fig. 2), where
91 they lay directly over the Paleozoic basement. Hence, there is no geological continuity between
92 the lower Triassic sandstones (LTS, Buntsandstein) and the Keuper sandstones that are
93 present beneath the centre of the basin. Finally, at the top of the Triassic sedimentary
94 succession, the Rhaetian sandstones (upper Keuper, Fig. 2) have been recognized in most
95 areas throughout the basin.

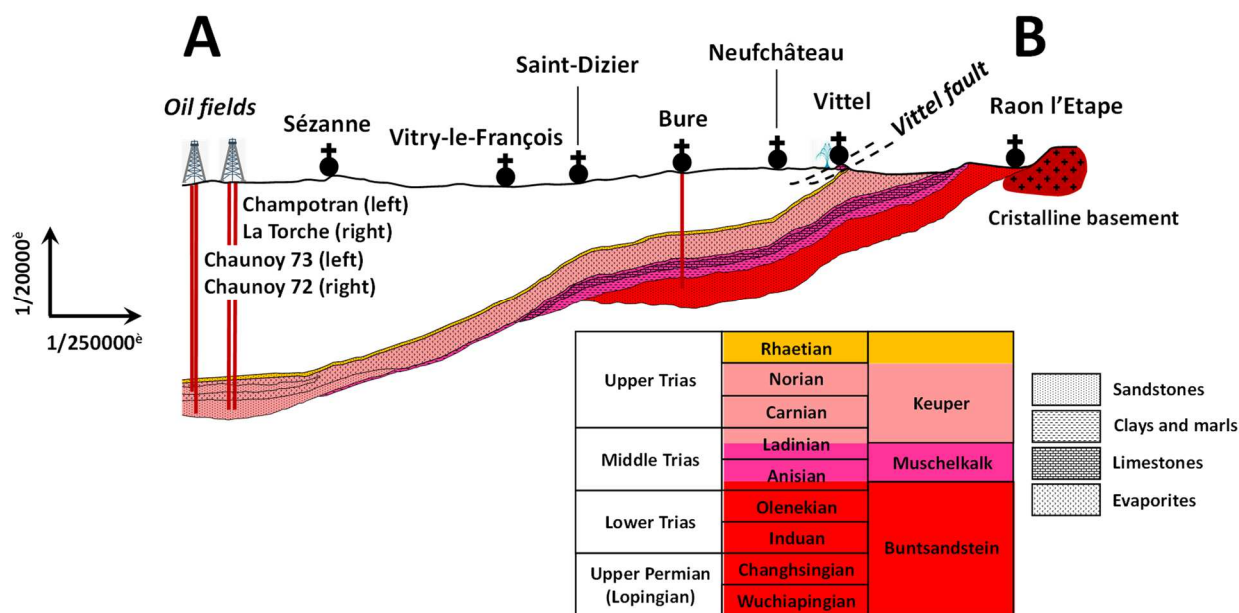
96 The triassic series are overlain by the jurassic deposits, which extend over the whole Paris
97 Basin and include the deepest aquifer overlying the Trias : the Dogger aquifer (mostly middle
98 Jurassic deposits).

99



100
 101 Figure 1 : Geographic map showing the location of the study area and its schematic geological
 102 background, with sampling points. The Bray-Vittel fault is represented in black. Red circles correspond to
 103 LTS waters, brown circles to Muschelkalk waters, and the blue circles to the Dogger springwater. Waters
 104 from the confined part of the LTS aquifer are marked by a bold black outline.

105



106
 107 Figure 2 : Schematic West to East cross-section of the eastern part of the Paris basin, from points A to B
 108 (Fig. 1), with schematic stratigraphy and lithology of the triassic deposits. Deep borehole EST 433 of the
 109 Bure area (Rebeix et al., 2011; Millot et al., 2011a, and those of the oil fields East of the Paris region
 110 (Millot et al., 2011b) have been represented. The cross-section has been drawn after the data available in
 111 Mégnien et coll. (1980) and in Gély, Hanot et coll. (2014).

112
 113 From a structural point of view, the study area is characterized by the presence of the Bray-
 114 Vittel fault (BVF, referred as “Vittel fault” in Fig. 2), which constitutes a major fault of the earth's
 115 crust and has to be regarded as a very important element for the deep structure of the
 116 sedimentary Paris Basin (Mégnien, 1980) (Fig. 1 ; Fig. 2).

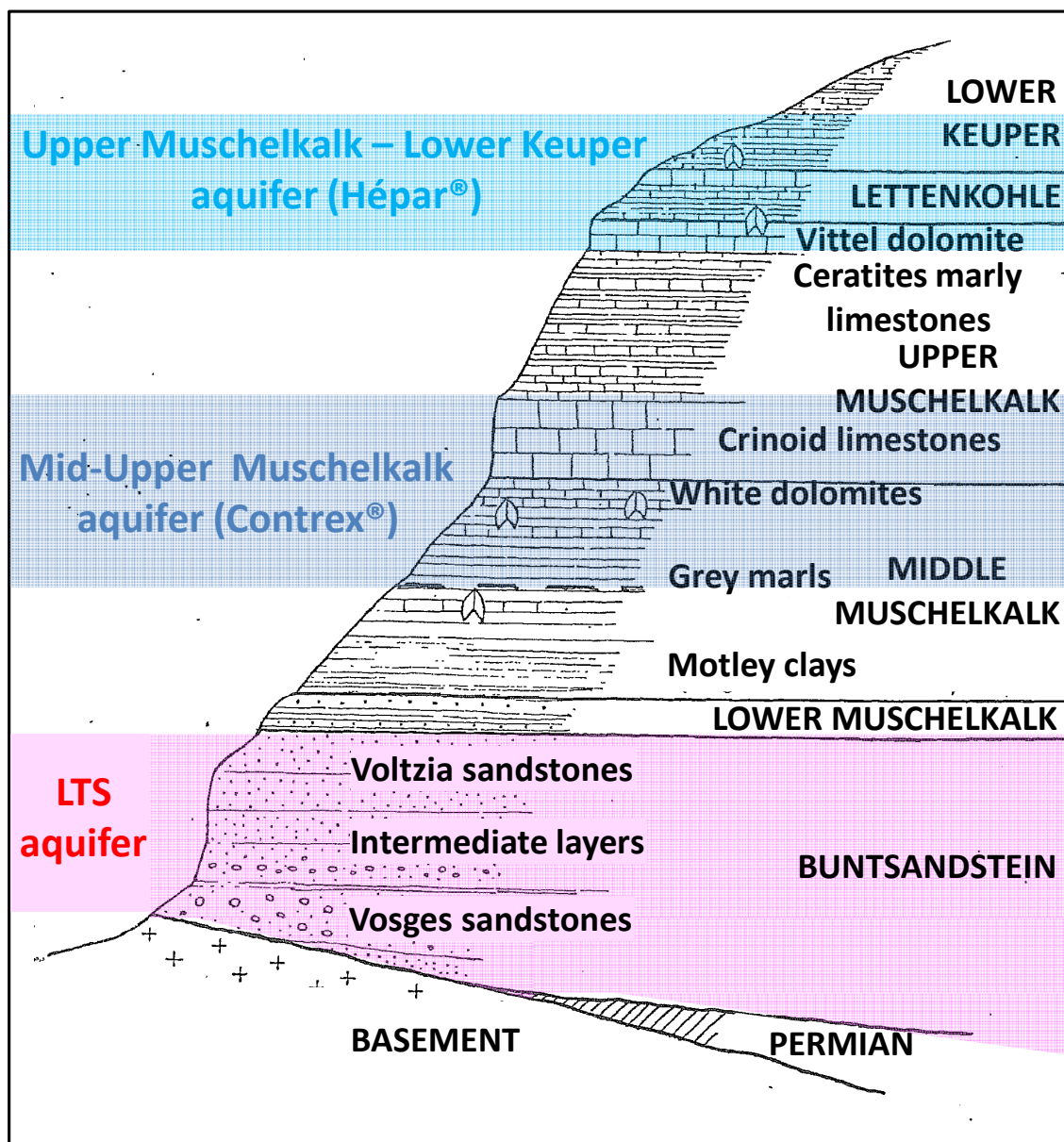
117 In the study area, the crystalline basement is made of granitic rocks South of the BVF (Minoux,
 118 1967 ; Marotel et Minoux, 1973). The lithological nature of the basement may be different North
 119 of the BVF, as the two variscan structural units are not identical (Mégnien, 1980). Permian
 120 series do not crop out south of the BVF (Marotel et Minoux, 1973), but they are probably
 121 present under younger lithologies, namely at Bulgnéville (Minoux, 1967). Where Permian is
 122 absent, the LTS lay directly over the basement. In contrast, Permian series have been
 123 described North of the BVF, near Mirecourt (Marotel et Minoux, 1975). The LTS (Buntsandstein)

124 are classically divided in 3 facies : (i) Vosges sandstones ; (ii) Intermediate, coarser layers and,
125 (iii) *Voltzia* sandstones. The lower Muschelkalk is constituted by red sandstones and clays. The
126 middle Muschelkalk includes motley clays, then grey dolomitic marls with evaporites, and finally
127 white dolomites with gypsum at their bottom. The upper Muschelkalk is made of crinoid
128 limestones, overlain by *Ceratites*-bearing marly limestones, and by the Vittel dolomite (Minoux,
129 1966; Marotel et Minoux, 1973) (Fig. 3).

130 Permian formations are not productive from an hydrologic point of view (Minoux, 1967 ; Marotel
131 et Minoux, 1973). In contrast, the three main facies of the LTS are aquifer formations, which
132 represent, at present, the main groundwater resource in this area (Fig. 3). The LTS aquifer
133 becomes confined at the southern limit of the study area. The lower Muschelkalk is partly
134 clayey, as well as the bottom layer of the middle Muschelkalk (heterogeneous clays). These
135 lithologies act as an aquiclude separating the LTS aquifer from that constituted by the overlying
136 upper facies of the middle Muschelkalk (grey marls and white dolomites, Fig. 3) and the base of
137 the upper Muschelkalk (crinoid limestones). This groundwater resource includes several mineral
138 springs, like the worldwide famous Great Source[®] at Contrexéville (Contrex[®] bottled water)
139 (Fourniguet, 2012 and references therein, Fig. 3). Mineralizing processes result probably from
140 the interaction of water with gypsum lithologies (Fourniguet, 2012). *Ceratites*-bearing marly
141 limestones separate the mineral water resource briefly described above from another which is
142 located in the upper layers of the upper Muschelkalk (Vittel dolomite) and extends up to the
143 bottom of the overlying Lettenkohle and lower Keuper lithologies. This mineral water resource
144 includes the famous Hépar[®] bottled water.

145

146



147
 148 Figure 3 : Schematic stratigraphic succession of the triassic series in the Vittel area (south of the BVF)
 149 with emphasis on the different aquifer levels (after Minoux, 1966).

150
 151 **3 – Sampling and analytical techniques**
 152 Fifteen waters were sampled in july 2011 and november 2012 (Fig. 1). Twelve waters come
 153 from the LTS aquifer, including two of them (point 1 : Etival-Clairefontaine and point 7:
 154 Relanges) in an unconfined context. Two samples are from the overlying, mid to upper
 155 Muschelkalk aquifer : Contrex Great Source® (point 13) and Le Bon Pré (point 14). Both are

156 very close to other points (9 : Frênes and 10 : Suriauville) where LTS waters were collected
 157 (Fig. 1) in order identify possible leakage processes. Finally, a springwater from the overlying
 158 Dogger aquifer was sampled (point 15 : Illoud), near the western end of the study area to get an
 159 outline of this deep aquifer overlying the triassic deposits.

160 Physical and chemical parameters (T°, pH, Eh, electrical conductivity, dissolved O₂) were
 161 measured directly in the field, and the alkalinity immediately once back from the field sampling
 162 campaign. Results are reported in Table 1, with the geographic location of samples.

163

Sample	Formation	T° C	pH	Eh (mV)	Dissolved O ₂ (%)	Conductivity 25°C (µS/cm)	Alkalinity (meq/l)
1 Etival-Clairefontaine	Lower Trias (unconfined)	10.7	6.78	179	87.0	237	1.72
2 Saint-Genest	Lower Trias (confined)	22.1	7.05	139	64.5	404	2.37
3 Rehaucourt	Lower Trias (confined)	11.5	7.07	181	45.3	1121	5.95
4 Poussay - Val d'Arol	Lower Trias (confined)	24.5	7.44	-1	2.5	614	3.42
5 Mirecourt	Lower Trias (confined)	20.7	7.99	330	93.7	337	2.18
6 Valfroicourt	Lower Trias (confined)	15.3	7.20	402	60.0	419	2.51
7 Relanges	Lower Trias (unconfined)	10.8	7.18	300	80.8	209	1.82
8 Vittel	Lower Trias (confined)	15.6	7.47	154	2.0	525	3.55
9 Frênes	Lower Trias (confined)	16.3	7.52	162	22.3	478	3.64
10 Suriauville	Lower Trias (confined)	15.4	7.58	171	1.0	526	3.71
11 Bulgnéville	Lower Trias (confined)	23.8	7.45	135	72.2	721	3.74
12 Norroy	Lower Trias (confined)	24.5	7.49	98	0.5	256	3.73
13 Contrex Great Source	Muschelkalk	12.2	7.14	252	1.3	2400	6.06
14 Le Bon Pré	Muschelkalk	11.3	7.26	375	19.0	702	6.72
15 Illoud	Dogger	9.7	7.06	170	100.0	434	4.05

164

165 Table 1 : Physical and chemical parameters for the fifteen water samples. Samples 13 to 15 were
 166 recovered
 167 from unconfined aquifers. Samples 1 to 4 and sample 15 were collected in July 2011, and samples 5 to 14
 168 in November 2012.

169

170 Concentrations in major cations (Ca, Mg, Na, K) were determined by at BRGM Orléans by
 171 Inductively Coupled Plasma Optical Emission Spectrometry (ICP-OES) on waters previously
 172 filtered at 0.45 µm and acidified at pH~2, in order to avoid element adsorption on the bottle
 173 walls, and also to prevent the development of bacterial flora. Major anions (Cl, Br, SO₄, NO₃)
 174 were analyzed on 0.45 µm filtered waters by ionic chromatography. Bicarbonate contents were
 175 derived from alkalinity. Si, As, B, Li, and Sr concentrations were measured on 0.45 µm filtered

176 and acidified waters on a X7 Quadrupole Inductively Coupled Plasma Mass Spectrometer (ICP-
 177 MS). Results are reported in Tables 2 and 3.

Sample	Formation	Ca (mg/l)	Mg (mg/l)	Na (mg/l)	K (mg/l)	HCO ₃ (mg/l)	NO ₃ (mg/l)	SO ₄ (mg/l)	Cl (mg/l)	Br (mg/l)	Si (mg/l)	As (µg/l)
1 Etival-Clairefontaine	Lower Trias (unconfined)	25.6	11.6	2.7	1.7	110	6.1	11.5	5.8	< 0.1	11.6	n.d.
2 Saint-Genest	Lower Trias (confined)	32.3	16.6	20.5	4.2	150	< 0.5	38.4	26.7	< 0.1	11.3	n.d.
3 Rehaucourt	Lower Trias (confined)	210.9	43.4	3.7	1.7	373	10.0	355.7	9.8	< 0.1	10.0	n.d.
4 Poussay - Val d'Arol	Lower Trias (confined)	29.4	11.6	82.8	7.0	210	< 0.5	50.7	67.6	0.9	12.4	n.d.
5 Mirecourt	Lower Trias (confined)	25.6	9.1	17.9	4.1	137	< 0.5	20.8	17.6	0.1	11.5	35.9
6 Valfroicourt	Lower Trias (confined)	40.7	9.6	18.2	3.4	156	1.0	48.3	18.3	0.1	10.6	33.9
7 Relanges	Lower Trias (unconfined)	28.8	3.3	1.6	1.8	112	0.6	2.7	2.3	< 0.1	7.9	15.1
8 Vittel	Lower Trias (confined)	66.8	13.1	6.5	3.2	220	< 0.5	74.6	3.7	< 0.1	8.2	25.2
9 Frênes	Lower Trias (confined)	58.2	13.5	9.8	3.2	216	< 0.5	61.5	5.7	< 0.1	7.7	22.9
10 Suriauville	Lower Trias (confined)	61.4	14.7	14.5	2.9	230	< 0.5	72.1	8.3	< 0.1	8.2	40.2
11 Bulgnéville	Lower Trias (confined)	95.6	19.0	13.7	5.0	234	< 0.5	179.0	6.8	< 0.1	9.7	30.3
12 Norroy	Lower Trias (confined)	86.9	8.3	379.9	14.3	239	< 0.5	436.0	402.0	4.8	10.8	30.9
13 Contrex Great Source	Muschelkalk	477.1	60.9	11.3	3.0	375	< 0.5	1223.0	5.8	< 0.1	11.3	0.60
14 Le Bon Pré	Muschelkalk	75.9	38.3	1.8	1.0	420	17.5	14.5	7.8	< 0.1	7.0	0.28
15 Illoud	Dogger	85.1	3.3	1.5	< 0.5	252	0.6	10.2	3.1	< 0.1	3.6	n.d.

178
 179 Table 2 : Major element data, and Br, Si, and As contents for the fifteen water samples. Analytical
 180 uncertainties are 5%.

181
 182 Oxygen and hydrogen isotopes were measured in the groundwaters by Isotope Ratio Mass
 183 Spectrometry (IRMS) using the equilibration method : H₂ for hydrogen and CO₂ for oxygen,
 184 respectively.
 185 Sulfur and oxygen isotopes of dissolved sulfates were first stabilized in the field using cadmium
 186 acetate, then filtered in the laboratory. Finally, sulfates were precipitated using barium chloride,
 187 and analyzed by Continuous Flow (CF)-IRMS.
 188 Sr and Li isotopes were measured on acidified and filtered waters. For B isotopes, waters were
 189 also filtered, but not acidified. Sr, Li, and B were extracted from the matrix using Sr Spec
 190 specific resin, 50WX12 cationic resin, and Amberlite IRA-743 selective resin, respectively.
 191 These techniques are detailed in Millot et al. (2011b). B and Sr have been analyzed by Thermal
 192 Ionization Mass Spectrometer (TIMS), on a Finnigan MAT 261 for B, and on a Finnigan MAT
 193 262 for Sr. Li was measured on a Thermo Neptune MC-ICPMS plasma source magnet mass
 194 spectrometer (Millot et al., 2011b). The isotopic data, together with corresponding element
 195 concentrations, are reported in Table 3.

196
 197

Sample	Formation	$\delta^{18}\text{O}$	δD	$\delta^{34}\text{S}_{\text{sulfates}}$	$\delta^{18}\text{O}_{\text{sulfates}}$	B ($\mu\text{g/l}$)	$\delta^{11}\text{B}$	Li ($\mu\text{g/l}$)	$\delta^7\text{Li}$	Sr ($\mu\text{g/l}$)	$^{87}\text{Sr}/^{86}\text{Sr}$
1 Etival-Clairefontaine	LTS (unconfined)	-8.3	-57.7	n.d.	n.d.	3.5	17.51 (11)	2.5	0.8	19	0.711234 (09)
2 Saint-Genest	LTS (confined)	-8.9	-62.8	n.d.	n.d.	19.4	12.45 (12)	32.8	5.2	177	0.711492 (06)
3 Rehaincourt	LTS (confined)	-8.0	-55.4	n.d.	n.d.	46.3	0.94 (18)	22.9	13.1	761	0.708191 (06)
4 Poussay - Val d'Arol	LTS (confined)	-9.8	-70.3	n.d.	n.d.	159.0	13.30 (14)	277.0	5.1	481	0.712710 (06)
5 Mirecourt	LTS (confined)	-9.3	-65.6	10.2	7.6	22.5	21.43 (04)	109.0	3.9	239	0.712959 (09)
6 Valfroicourt	LTS (confined)	-8.5	-58.4	14.7	9.4	84.1	-3.48 (06)	151.0	4.8	433	0.713064 (09)
7 Relanges	LTS (unconfined)	-8.6	-58.8	10.1	6.6	9.8	-16.08 (09)	11.8	0.8	36	0.713216 (09)
8 Vittef	LTS (confined)	-8.5	-58.3	15.2	10.1	33.3	-6.92 (03)	77.9	2.5	626	0.711662 (09)
9 Frénes	LTS (confined)	-8.4	-57.7	14.6	9.1	43.4	1.32 (05)	86.6	4.2	523	0.712031 (08)
10 Suriauville	LTS (confined)	-8.4	-57.9	12.1	8.8	66.1	-0.47 (05)	99.3	5.1	569	0.712638 (10)
11 Bulgnéville	LTS (confined)	-8.7	-60.3	16.9	11.0	52.1	-4.56 (06)	128.0	3.8	1240	0.712224 (09)
12 Norroy	LTS (confined)	-9.3	-66.2	15.4	8.3	1171.0	-2.71 (05)	1768.0	6.5	3455	0.713079 (08)
13 Contrex Great Source	Mid-Upper Muschelkalk	-8.1	-55.7	18.8	14.6	295.0	-5.28 (06)	101.0	7.5	4983	0.708866 (09)
14 Le Bon Pré	Mid-Upper Muschelkalk	-8.2	-55.9	-4.3	3.6	9.3	-9.38 (04)	14.2	-0.4	63	0.710133 (07)
15 Iloud	Dogger	-7.8	-53.1	n.d.	n.d.	4.1	15.87 (16)	0.5	5.6	77	0.707834 (08)

199
200 Table 3 : Isotopic data and corresponding element concentrations for the fifteen waters samples. Errors in
201 parenthese are reported as 2σ . O, D, S, B and Li isotopic signatures are reported as conventional δ
202 units :

203 $\delta_{\text{sample}} = (R_{\text{sample}}/R_{\text{standard}} - 1) \times 1000$, where R is the isotopic ratio. Standards are the Standard Mean
204 Oceanic Water (SMOW) for O and D, the Canyon Diablo Troilite (CDT) for S, NIST SRM-951 for B and
205 NIST SRM-8545 for Li. Uncertainties on the delta values are estimated at 0.1‰ for $\delta^{18}\text{O}$, 0.8 ‰ for δD ,
206 0.3‰ for $\delta^{34}\text{S}$, 0.5‰ for $\delta^7\text{Li}$ and 0.3‰ for $\delta^{11}\text{B}$. Uncertainties on the concentrations are 5%.

207
208 Carbon isotopic analyses, as well as ^{14}C activities measurements were done by Beta Analytic
209 inc. CO_2 was extracted under vacuum and purified, then samples were divided in two aliquots.
210 The isotopic composition was measured by IRMS, and ^{14}C activities by AMS (mass
211 spectrometry coupled with a particle accelerator). Results are reported in Table 4.

212

213

214

215

216

Sample	Formation	$\delta^{13}\text{C}$	Act. ^{14}C pCM	Age ^{14}C BP conv.	Pearson	Fontes / Garnier	Evans	Eichinger
1 Etival-Clairefontaine	Lower Trias (unconfined)	-15.8	60.6	4030	1795	3835	1770	0
2 Saint-Genest	Lower Trias (confined)	-8.9	17.1	14170	7484	7427	7047	8652
3 Rehaucourt	Lower Trias (confined)	-14.3	71.2	2730	0	1261	0	0
4 Poussay - Val d'Arol	Lower Trias (confined)	-13.0	2.4	29910	26799	27722	26573	26514
5 Mirecourt	Lower Trias (confined)	-14.3	10.7	17950	15299	16649	15165	14367
6 Valfroicourt	Lower Trias (confined)	-16.4	34.3	8590	6802	8781	6753	4937
7 Relanges	Lower Trias (unconfined)	-18.9	71.1	2740	1949	4551	1940	0
8 Vittel	Lower Trias (confined)	-15.6	38.8	7600	5369	7176	5307	3769
9 Frênes	Lower Trias (confined)	-15.5	37.3	7920	5642	7402	5573	4106
10 Suriauville	Lower Trias (confined)	-15.5	33.3	8830	6580	8372	6518	5002
11 Bulgnéville	Lower Trias (confined)	-15.3	24.7	11240	8942	10419	8811	7824
12 Norroy	Lower Trias (confined)	-10.6	1.1	36490	31630	31678	31266	32249
13 Contrex Great Source	Muschelkalk	-12.5	56.5	4580	431	1434	358	0
14 Le Bon Pré	Muschelkalk	-13.9	83.1	1490	0	0	0	0
15 Illoud	Dogger	-14.1	99.1	70	0	0	0	0

217

218 Table 4 : $\delta^{13}\text{C}$, ^{14}C activities and calculated ages. The delta 0 for C isotopic signatures is the Pee Dee
219 Belemnite (PDB). Conventional ages were calculated with an initial activity of 100% of modern carbon.
220 The four applied correction models (Pearson and Handshaw, 1970; Fontes and Garnier, 1979; Evans et
221 al., 1979; Eichinger, 1983) are considered to be the most suitable models in the case of the LTS aquifer
222 (Celle-Jeanton et al., 2009).

223

224 4 – Results and discussion

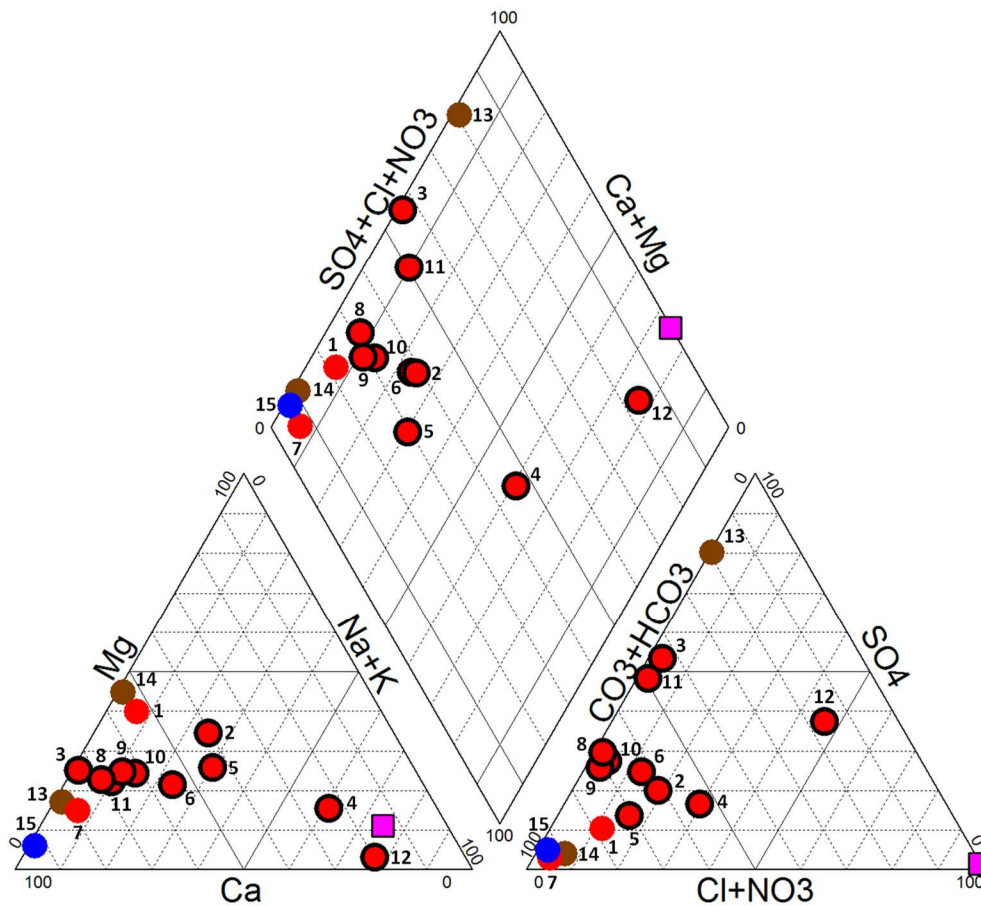
225

226 4.1. Geochemical facies of the groundwaters

227 Major element data (Tab. 2) allow to determine the geochemical facies of sampled waters (Fig.
228 4). Considering LTS groundwaters, the two samples collected in the unconfined part of the
229 aquifer (Etival-Clairefontaine-1 and Relanges-7) display clearly a calcium-bicarbonate facies,
230 groundwater 1 having in addition a slight magnesian fingerprint. Overall, LTS waters sampled in
231 the confined aquifer have the same facies. Two waters (Rehaucourt-3 and Bulgnéville-11)
232 display a slight shift towards a sulfate geochemical facies (Fig. 4). Finally, waters from Norroy-
233 12 and Poussay-Val d'Arol-4 have a alkaline facies (Fig. 4), shifting towards the Triassic brines.
234 Both groundwaters displays also slightly warmer temperatures (24.5°C) and a relatively low Eh :
235 98 and -1 mV, respectively (Tab. 1).

236

237



238
 239 Figure 4 : Piper diagram for the fifteen sampled waters. Red circles correspond to LTS waters, brown
 240 circles to Muschelkalk waters, and the blue circles to the Dogger springwater. Waters from the confined
 241 part of the LTS aquifer are marked by a bold black outline. The point of the triassic brines (Millot et al.,
 242 2011a) is plotted as a pink square.

243
 244 A previous study, focussed on two decades of LTS aquifer overpumping has been published by
 245 Celle-Jeanton et al. (2009). The study area is located North of that of this study. It includes
 246 major and trace element data, hydrogen, oxygen and carbon stable isotopes, and finally ¹⁴C
 247 dates. The geochemical characteristics of the LTS waters are in agreement with those
 248 measured by Celle-Jeanton et al. (2009). However, the dataset of these authors includes much

249 more waters influenced by the Cl – alkaline end-member, since it covers the whole LTS aquifer,
250 including the north of the Lorraine area, whereas the present study mainly focusses on the
251 southern end of the aquifer. Celle-Jeanton et al. (2009) also pointed out that these geochemical
252 characteristics are related to the dissolution of evaporites, that was enhanced since 1979.
253 The two waters from the Mid-Upper Muschelkalk aquifer display very different characteristics.
254 Sample 13 corresponds to the Great Source® at Contrexéville which is clearly a sulfate water,
255 with Ca as the major cation (Fig. 4). In contrast, sample 14 (Le Bon Pré) is less mineralized
256 (Tab. 1) and displays a Ca bicarbonate facies. Finally, the spring water recovered at Illoud
257 (sample 15) is purely calcic and bicarbonated (Fig. 4).
258 LTS waters display high As concentrations, especially in the confined part, as high as 40 µg/l
259 (Tab. 2). Such contents are clearly higher than drinking water regulations (10 µg/l). In contrast,
260 Muschelkalk waters are As – free (Tab. 2). The As present in the LTS waters does not derive
261 from an anthropic pollution, and has a geogenic origin, possibly resulting from hydrothermal
262 processes, as it has been evidenced in other sites (e.g.; Aiuppa et al., 2003; 2006; Rowland et
263 al., 2011 + Réf. Romain).

264

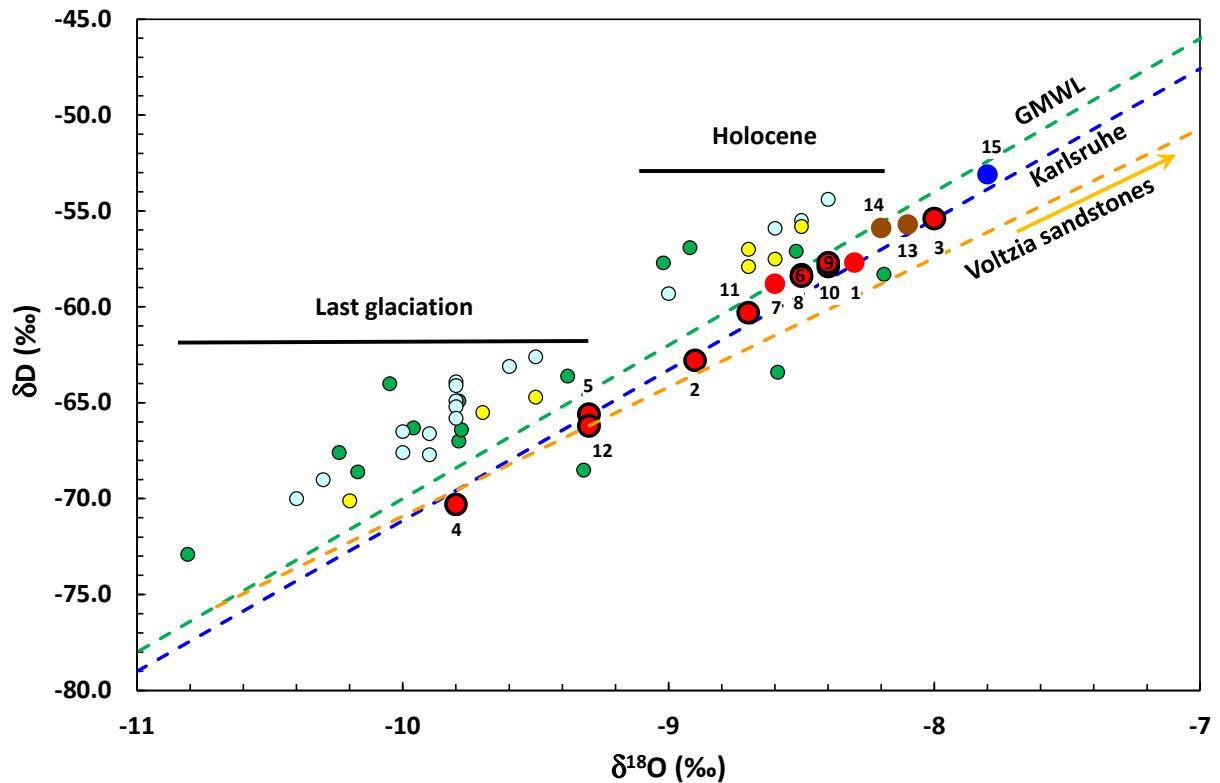
265 **4.2. The origin of LTS waters**

266

267 4.2.1. Meteoric waters

268 Data reported in Figure 5 show that all data points follow a linear trend, close to the Global
269 Meteoric Water Line, and even closer to the local meteoric line of Karlsruhe (Celle-Jeanton et
270 al., 2009). The oxygen isotopic signature of the Karlsruhe rainwater is – 8.2‰. The rainwaters
271 from the study area should be similar or slightly lower in its northeastern part (Millot et al.,
272 2010a). Most LTS waters plot around an average value of -8.5‰ for $\delta^{18}\text{O}$, and -60‰ for δD ,
273 indicating that such isotopic compositions are characteristic of present-day, meteoric waters.

274



276

277 Figure 5 : δD vs. $\delta^{18}O$ diagram for the studied waters. Red circles correspond to LTS waters, brown
 278 circles to Muschelkalk waters, and the blue circle to the Dogger springwater. Waters from the confined
 279 part of the LTS aquifer are marked by a bold black outline. Data from Blavoux and Olive (1981) are
 280 reported as yellow circles (southern part of the aquifer) and as blue circles for the northern part. Data
 281 from Celle-Jeanton et al. (2009) are reported as green circles. The global meteoric line of Craig (1961)
 282 has been reported in green, the local line of Karlsruhe (Celle-Jeanton et al., 2009) in blue. Current stable
 283 isotope signatures of Karlsruhe rainwater are $\delta^{18}O = -8.1\text{‰}$, $\delta D = -57.2\text{‰}$ (Celle-Jeanton et al., 2009).
 284 The orange dashed line emphasizes the influence of the triassic brines. Current stable isotope signatures
 285 are $\delta^{18}O = -2.1\text{‰}$, $\delta D = -17.8\text{‰}$ (Rebeix et al., 2011).

286

287 Muschelkalk waters (Contrex Great Source[®]-13 and Le Bon-Pré-14) plot also within the domain
 288 of the average recent LTS waters. The Dogger water from Illoud (15), located westwards, is
 289 even less depleted in heavy isotopes (Fig. 5), in agreement with the mean isotopic signatures of
 290 rainwaters in France (Millot et al., 2010a).

291 Data published previously on LTS waters (Blavoux and Olive, 1981; Celle-Jeanton et al., 2009)
292 follow more or less the GMWL (Fig. 5), although plotting slightly higher than those of the present
293 study, including waters from the southern part of the aquifer.

294 Stable isotopes of the water molecule allow estimating the age of recharge, the lowest delta
295 values corresponding to the coldest climatic conditions. Three LTS waters exhibit lower isotopic
296 signatures : Mirecourt (5), Norroy (12) and especially Poussay-Val d'Arol (4). Previous studies
297 from Blavoux and Olive (1981) and Celle-Jeanton et al. (2009) have emphasized a clear
298 correlation between oxygen isotopic signatures and ^{14}C ages. The age of water recharge is
299 shown in Figure 5. Considering the present dataset, this indicates that waters from Poussay-Val
300 d'Arol (4), Mirecourt (5) and Norroy (12) would derive from an older recharge under colder
301 climatic conditions, during the last glaciation, which would agree with hydrological parameters
302 (Vaute et al., 2013).

303

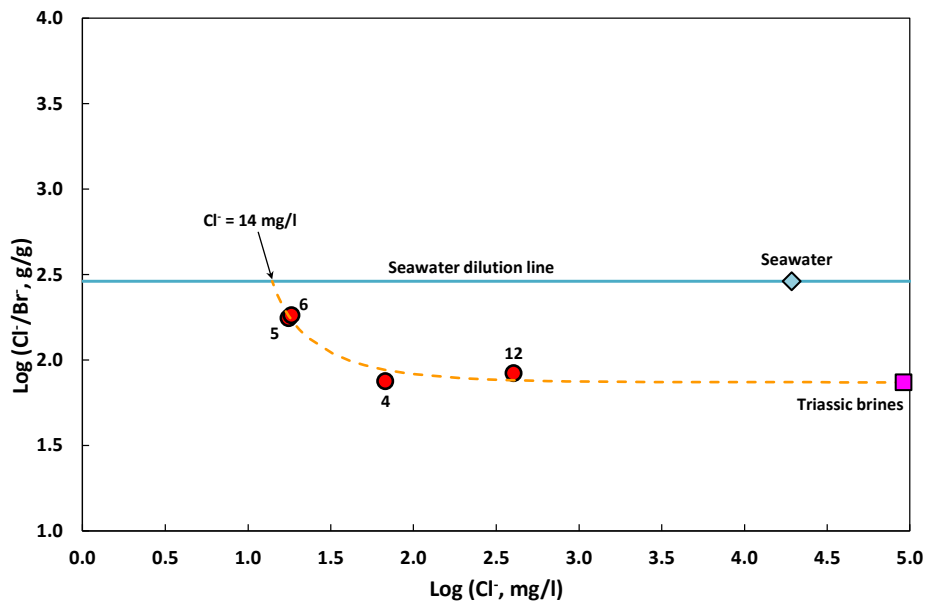
304 4.2.2. Lower Triassic brines

305 Among all LTS waters, Norroy (12) is the most mineralized water, with a TDS of 6907 mg/l (Tab.
306 2). It displays a Cl – Na geochemical facies, as shown by the Piper diagram (Fig. 4). This water
307 is clearly the most evolved relative to recharge water.

308 The alkaline / chloride end-member is thought to refer most probably to brines with
309 characteristics similar to the than waters from the *Voltzia* sandstones, towards the center of the
310 Paris basin (Milot et al., 2011a; Rebeix et al., 2011). These brines are located in the upper layer
311 of the Buntsandstein series, and should be distinguished from the oil-bearing geothermal
312 Keuper brines of the center of the Paris basin (e.g.; Matray et al., 1989; Fig. 2).

313 The involvement of such brines is illustrated in Figure 6, coupling chloride and bromide data
314 (Matray et al., 1989). The present-day seawater has a Cl/Br ratio of 289 in atomic weight. This
315 ratio remains constant in marine aerosols that are present in meteoric waters (considering that
316 there is no other source of Cl and Br involved). In Figure 6, it is noticeable that the four waters
317 which can be reported on the diagram (Br content higher than the quantification limit, Tab. 2)

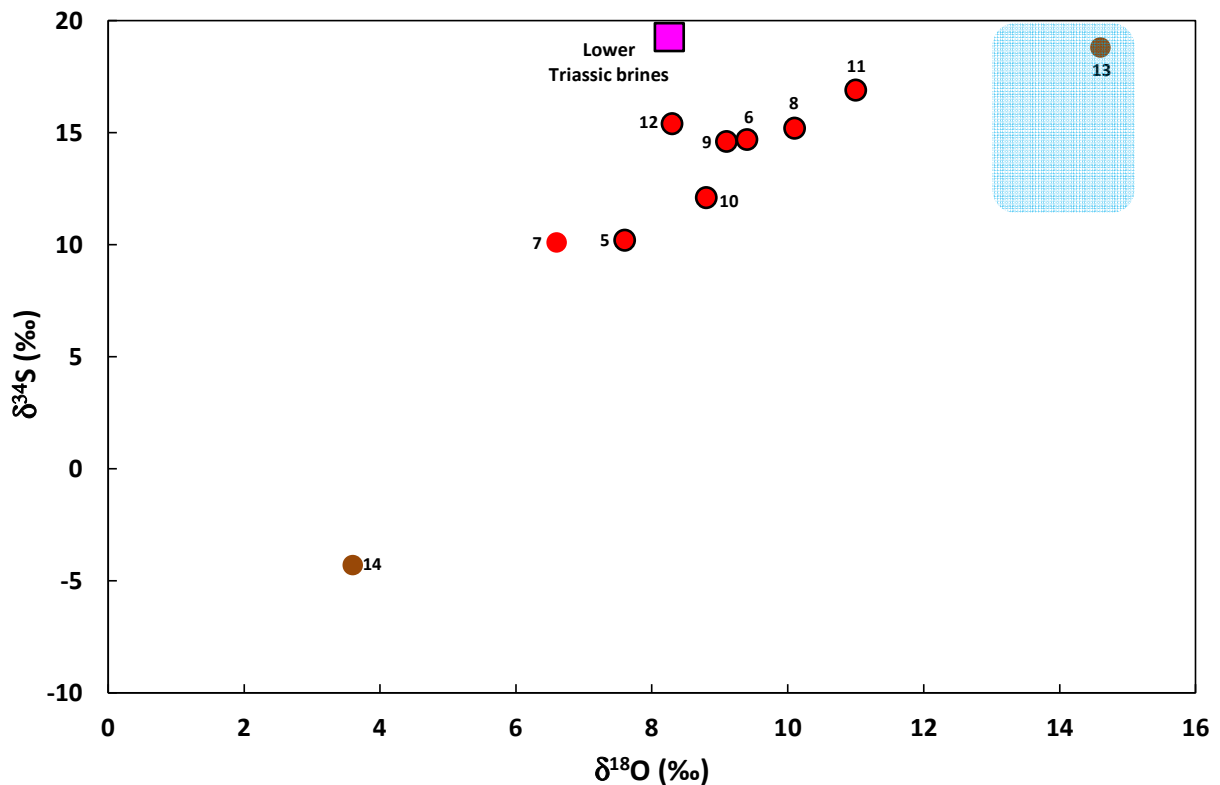
318 plot on a mixing curve, away from the seawater dilution line : Mirecourt (5),Valfroicourt (6),
319 Poussay-Val d'Arol (4) and Norroy (12). They all record the influence of brines having a Cl-Br
320 geochemical signature similar to that of saline waters recovered from the *Voltzia* sandstones, in
321 the transposition zone of the Bure radioactive waste repository site (Rebeix et al., 2011). The
322 second end-member represents the intersection between the mixing curve and the seawater
323 dilution line. It corresponds to a chloride content of 14 mg/l (Fig. 6). All waters that cannot be
324 plotted on the diagram display chloride contents lower than this value (Tab. 2). The only
325 exception is the Saint-Genest water (2), but it should be stressed that it is located East of the
326 Vittel – Contrexéville area and could have a different history. (Fig. 1). Another argument in favor
327 of a contamination by triassic brines comes from the $\delta^{18}\text{O}$ - δD diagram (Fig. 5). It can be
328 noticed that, although remaining close to the GMWL, the Norroy water (12) plots slightly under
329 this line. The straight line defined by the Norroy datapoint and the isotopic compositions of the
330 triassic brines (-2.11‰ for $\delta^{18}\text{O}$ and -17.8‰ for δD ; Rebeix et al., 2011) is reported in orange in
331 Figure 5. It is also noticeable that Poussay-Val d'Arol (4) and Mirecourt (5) waters plot on this
332 orange line. This suggests that oxygen and hydrogen isotopic compositions in some waters
333 (Norroy-12, Mirecourt-5, Poussay-Val d'Arol-4) may be higher to that they would be if recording
334 only climatic variations, resulting in addition from the slight influence of the lower triassic brines.
335



336
 337 Figure 6 : Log (Cl⁻/Br⁻) vs. Log (Cl⁻) diagram for the studied waters. Red circles correspond to LTS waters.
 338 Waters from the confined part of the LTS aquifer are marked by a bold black outline. The seawater
 339 dilution line is plotted in blue, and the seawater – brine mixing curve is plotted in orange. The mixing
 340 “curve” is actually a straight line, mathematically. It appears as a curve on the diagram due to the log
 341 scale of the axes.

342
 343 Sulfur and oxygen isotopes of dissolved sulfates (Tab. 3, Fig. 7) also indicate a possible
 344 fingerprint of triassic saline waters for the most concentrated water (Norroy-12), in agreement
 345 with Figures 5 and 6. The other groundwaters having highly positive sulfur isotopic signatures
 346 rather reveal the likely influence of Muschelkalk groundwaters similar to that of the Great
 347 Source[®] spring water of Contrexéville (13), whose isotopic signature of dissolved sulfates
 348 originate from the marine evaporites (gypsum) that are present in the aquifer. The groundwater
 349 from Relanges (7), which can be considered as representative for recharge waters (Vaute et al.,
 350 2013) has the less positive O and S isotopic signature of all LTS waters (Fig. 7). Hence, the
 351 trend emphasized by LTS waters data probably record the variable influence of gypsum
 352 dissolution.

353 Muschelkalk water from Le Bon Pré (14) does contain nitrates (17.5 mg/l, Tab. 2), very probably
 354 coming from sub-surface anthropic pollution (fertilizers). This groundwater also displays very
 355 low oxygen and sulfur isotopic signatures that probably result from surficial, sulfide oxydation
 356 processes (Berner, 1971) (Fig. 7).
 357

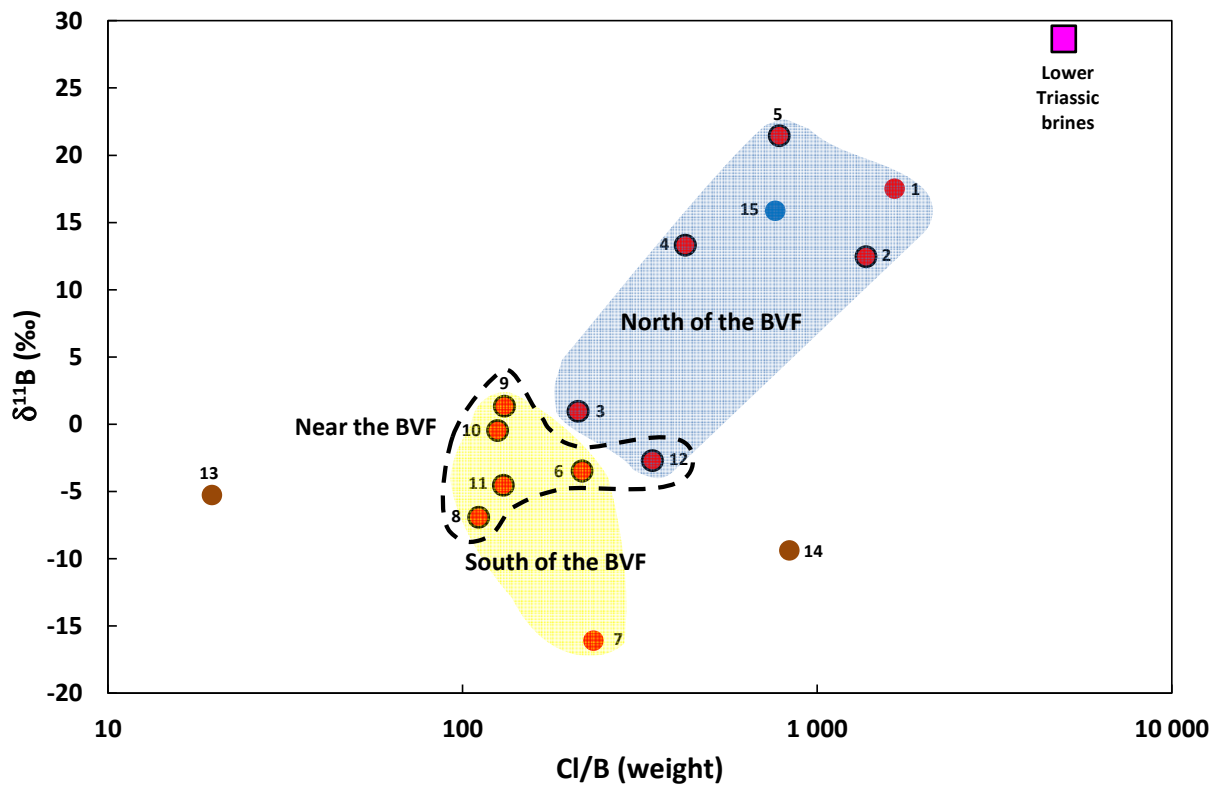


358
 359 Figure 7 : $\delta^{34}\text{S}$ vs. $\delta^{18}\text{O}$ diagram from dissolved sulfates for the studied waters. Red circles correspond to
 360 LTS waters and brown circles to Muschelkalk waters. The light blue field corresponds to the isotopic
 361 signature of triassic marine evaporites (Claypool et al., 1980). The value of lower triassic brines is derived
 362 from Rebeix et al. (2011).
 363

364 4.3. Dissolution processes and clay – water interaction

365 Four of the six LTS groundwaters located East of the study area and North of the BVF (Fig. 1) :
 366 Saint-Genest (2), Poussay Val d'Arol (4) and Mirecourt (5), have $\delta^{11}\text{B}$ higher than 10‰ and plot
 367 close to the corresponding recharge water (Etival-Clairefontaine-1) on a Cl/B - $\delta^{11}\text{B}$ diagram

368 (Fig. 8). The influence of the saline groundwaters of the *Voltzia* sandstones (Fig. 8) cannot be
 369 ruled out, although there is no further clear argument in favor of this hypothesis.
 370 In contrast, the other LTS waters, West of the study area and South of the BVF, cluster around
 371 a $\delta^{11}\text{B}$ slightly lower or close to 0‰, with Cl/B ratios between 100 and 400 (Tab. 2, Tab. 3, Fig.
 372 8). Once again, the corresponding recharge waters (Relanges-7) plot within this domain (Fig. 8).
 373



374
 375 Figure 8 : $\delta^{11}\text{B}$ vs. Cl/B ratio mixing diagram. Red circles correspond to LTS waters, brown circles to
 376 Muschelkalk waters, and blue circles to the Dogger springwater. Waters from the confined part of the LTS
 377 aquifer are marked by a bold black outline. Cl and B concentrations, and $\delta^{11}\text{B}$ for the triassic brines come
 378 from Millot et al. (2011a). Groundwaters plotting within the dashed field were sampled near the BVF,
 379 whether North and South (Fig. 1).
 380
 381 The groundwater from Norroy (12), located North of the BVF, also plots within this domain. For
 382 this sample, no influence of the saline waters from the *Voltzia* sandstones can be evidenced

383 from boron isotopes, unlike for sulfur and oxygen isotopes of dissolved sulfates. Similarly, one
384 would have expected a high $\delta^{11}\text{B}$ value of the Great Source® Muschelkalk mineral water of
385 Contrexéville (13) since its oxygen and sulfur isotopic characteristics derive from the dissolution
386 of gypsum evaporites (Fig. 7).

387 Such low boron isotopic signatures could be due to the interaction with clay materials. However,
388 desorption of exchangeable boron of argillaceous minerals would result in both higher $\delta^{11}\text{B}$ and
389 B concentrations in the groundwater (Pennisi et al., 2006). Hence this hypothesis does not
390 seem to be supported by the data (Fig. 8). In addition, argillaceous layers are very scarce in the
391 Buntsandstein sandstones. Alternatively, recharge waters (Etival North of the BVF, and
392 Relanges South of the BVF) having respectively the highest and the lowest $\delta^{11}\text{B}$, Cl/B and boron
393 isotopic signatures of LTS waters could result from the dissolution of boron having a low $\delta^{11}\text{B}$,
394 which would explain both the lowering of the two Cl/B ratios and the comparable $\delta^{11}\text{B}$ (from -7
395 to +2 ‰, Tab. 3) of the LTS waters close to the BVF (Fig. 8). This boron could originate from the
396 two Muschelkalk waters, which have appropriate $\delta^{11}\text{B}$, from -9 to -5 ‰ (Tab. 3). However, their
397 Cl/B ratios do not match the data (Fig. 8). For these two Muschelkalk waters, the hypothesis of
398 interaction processes with clay minerals is straightforward, as the Muschelkalk aquifer includes
399 several disseminated clay layers (Fig. 3).

400 The LTS groundwater from Rechaincourt (3) displays a boron isotopic signature that is drastically
401 lower than in the 4 other samples from the northeastern part of the study area. It is coupled with
402 a Sr isotopic composition significantly lower than those of the other groundwaters from this area
403 (Tab. 3). As this sample contains nitrates, a possible explanation calls for the influence of
404 mineral fertilizers, which are known to display boron isotopic values that may be very low
405 (Kloppmann et al., 2005 ; Widory et al., 2005), and Sr isotopic ratios as low as 0.7083 (Négre
406 and Deschamps, 1996), very close to of the groundwater of Rechaincourt (3) (Tab. 3). Sample Le
407 Bon Pré-14 from the Muschelkalk aquifer also contains significant amounts of nitrates (Fig. 2).

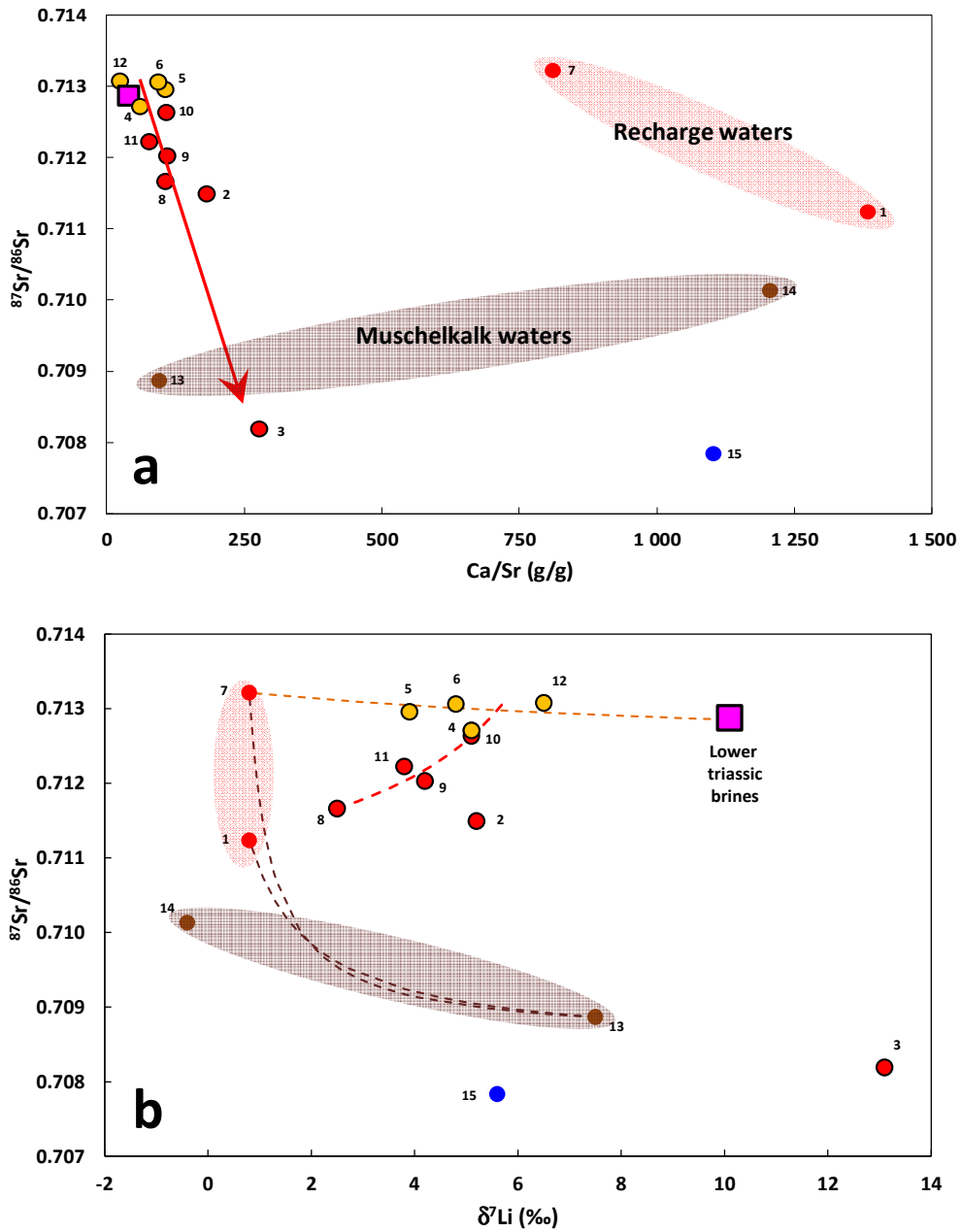
408 Its low $\delta^{11}\text{B}$ is thus fully compatible with the influence of fertilizers through sub-surface waters.
409 This could provide a alternative valuable explanation for its $\delta^{11}\text{B}$.
410 Finally, the water recovered from the Dogger aquifer (Illoud-15) displays a low Sr isotopic ratio
411 (Tab. 3) and a high $\delta^{11}\text{B}$, in respective agreement with the characteristics of this aquifer that
412 corresponds to Dogger marine limestones : 0.7073 (Rebeix et al., 2011) and from +15 to +30‰,
413 (Millot et al., 2011a).

414

415 **4.4. Water mixing – Leakage processes**

416 Groundwaters from Poussay (4), Mirecourt (5), Valfroicourt (6) and Norroy (12) have been found
417 to record the influence of the triassic brines from the upper layer of the LTS (*Voltzia*
418 sandstones), as demonstrated from halogen concentrations (Fig. 6). All LTS waters display Sr
419 isotopic compositions that are higher than 0.71, typical of siliceous sedimentary aquifers (e.g.;
420 Millot et al., 2011a). When plotted on a Ca/Sr – $^{87}\text{Sr}/^{86}\text{Sr}$ mixing diagram (Fig. 9a), these four
421 datapoints cluster around that of the triassic brines. Five of the six other waters from the
422 confined LTS aquifer seem to define a linear trend towards a hypothetical end-member having a
423 relatively low $^{87}\text{Sr}/^{86}\text{Sr}$ ratio and conversely a higher Ca/Sr elemental ratio (Fig. 9a). This end-
424 member cannot be related to recharge waters, which display Ca/Sr elemental ratios that are
425 much too high. These Ca/Sr ratios are unlikely to result from water/rock interaction, as it would
426 involve a huge lowering of this ratio, by half an order of magnitude, though preserving the linear
427 trend.

428



429
 430 Figure 9 : (a) $^{87}\text{Sr}/^{86}\text{Sr}$ vs. Ca/Sr mixing diagram. Red circles correspond to LTS waters, except that
 431 waters 4, 5, 6 and 12 have been distinguished from the others of the confined LTS aquifer by a orange
 432 colour. Brown circles correspond to Muschelkalk waters and the blue circles to the Dogger springwater.
 433 Data of the triassic brines are derived from Rebeix et al. (2011).
 434 (b) $^{87}\text{Sr}/^{86}\text{Sr}$ vs. $\delta^7\text{Li}$ mixing diagram. Same legend than in Figure 9a. For the triassic brines, Li data are
 435 from Millot et al. (2011b) and Sr data from Rebeix et al. (2011). The red mixing curve has been calculated
 436 with the characteristics of the Vittel water (datapoint n°8) and an "average" value of waters 4,5,6 and 12
 437 ($\text{Sr} = 430 \mu\text{g/l}$, $^{87}\text{Sr}/^{86}\text{Sr} = 0.713$; $\text{Li} = 150 \mu\text{g/l}$, $\delta^7\text{Li} : 5.7\text{‰}$).

438 Groundwaters from the overlying Muschelkalk aquifer could be adequate end-members,
439 considering their Sr isotopic composition (Fig. 9a), but none of the two Ca/Sr ratios measured in
440 these waters can fit the data. However, as they are very different from one to the other, the
441 range of Ca/Sr ratios in the Muschelkalk waters should be also very large. Hence, a hypothetical
442 Muschelkalk water having an intermediate Ca/Sr ratio could constitute an adequate end-
443 member. Alternatively, the groundwater from Rechaincourt (3), which is probably influenced by
444 anthropic activities (see above), possesses a Sr isotopic ratio and Ca and Sr concentrations
445 which make this water another possible end-member (Fig. 9a).

446 Thus, considering the very different Ca/Sr ratios of the two Muschelkalk groundwaters, there are
447 two possible end-members : (i) LTS groundwaters, whose geochemical and isotopic signatures
448 would be modified by anthropic inputs (Rechaincourt water – 3) or : (ii) waters from the overlying
449 Muschelkalk aquifer with a Ca/Sr ratio intermediate between the Great Source® (13) and Le Bon
450 Pré (14) waters.

451 The behavior of Li isotopes in groundwaters is still a matter of debate. Li isotopes may be in
452 some cases considered as conservative regarding water/rock interaction processes (Hogan and
453 Blum, 2003 ; Négrel et al., 2010 ; Millot et al., 2011a ; Meredith et al., 2013). In contrast, other
454 studies have concluded that Li isotopes may fractionate in aquifer systems as a function of
455 temperature (Millot and Négrel, 2007 ; Millot et al., 2007 ; 2010b). $\delta^7\text{Li}$ tends to decrease with
456 increasing temperatures. However, there are only slight variations in temperature (from 11.5 to
457 24.5°C) for confined LTS waters (Tab. 1). Furthermore, there is no negative correlation between
458 temperatures and Li isotopic signatures for LTS waters in this area. Hence, under the
459 hypothesis that no significant Li isotopic fractionation occurs during water-rock interaction,
460 coupling Sr and Li isotopes (Fig. 9b) may allow to better constrain the LTS aquifer system. Two
461 mixing trends may be emphasized. Firstly, groundwaters from Mirecourt (5), Valfroicourt (6) and
462 Norroy (12), this is to say three of the four samples plotting away from the seawater dilution line
463 in Figure 6, plot more or less along a mixing curve between the *Voltzia* sandstones brines and

464 the recharge water of Relanges (7). This end-member displays a Li isotopic signature ($\delta^7\text{Li} =$
465 0.8‰ , Tab. 3) similar to that of the upper continental crust ($0\text{‰} \pm 2$; Teng et al., 2004), whereas
466 its Sr isotopic ratio (0.7132, Tab. 3) is fully compatible with siliceous materials (triassic
467 sandstones). It is noticeable that the other recharge water at Etival-Clairefontaine (1) has the
468 same $\delta^7\text{Li}$ and a high Sr isotopic ratio (> 0.711 , Tab. 3), although slightly lower than that of
469 Relanges. Calculated contributions of the brine end-member are in any case extremely low ($<$
470 1‰).

471 Considering the groundwaters defining the linear mixing trend in Figure 9a (in red), the four
472 coming from the Vittel-Contrexéville area (this is to say apart from Saint-Genest-2 and
473 Rehaucourt-3 waters), and also the Poussay-Val d'Arol (4) water, plot on another mixing curve
474 (in red) in Figure 9b. The first potential end-member would have geochemical characteristics of
475 a groundwater originating from a mixture between the lower triassic brines and the recharge
476 water of Relanges (7) (orange curve on Figure 9b). The second end-member could correspond
477 to the other recharge water (Etival-Clairefontaine-1). However, this is in clear contradiction with
478 Figure 9a. Thus, if we assume that neither the Li isotopic signature nor the Ca/Sr ratio are
479 affected significantly by water/rock interaction processes, another end-member is required to
480 interpret the data.

481 In the light of sulfur and oxygen isotopes of dissolved sulphates (Fig. 7), this end-member
482 should record the influence of the groundwaters from the overlying Muschelkalk aquifer.
483 However, based on the two samples from this dataset, a pure Muschelkalk end-member cannot
484 fit the data, as their Sr isotopic compositions are too low (Fig. 9b). Hence, it may be related to a
485 mixture between Muschelkalk waters and recharge waters (Fig. 9b). Simple mixing curves
486 between the Great Source® (sample 13) mineral water and the two recharge waters have been
487 calculated and plotted as brown dashed curves. The LTS waters following the red curve are
488 thus compatible with a two end-member mixing, featuring a recharge/meteoric waters very
489 slightly influenced by triassic brines, and, as the second end-member, a mixture of

490 recharge/meteoric waters and Muschelkalk groundwaters. This indicates the existence of
491 leakage processes between the two aquifers in the western part of the study area.

492 Apart from the groundwater from Rechaincourt (3), which was shown to have specific
493 characteristics, it should be noticed that the groundwater from Saint-Genest (2) does not follow
494 the mixing curve in Figure 9b. Thus, there is no evidence for such leakage processes in the
495 eastern part of the study area (Fig.1)

496

497 **4.5. Residence time – Flowing velocities**

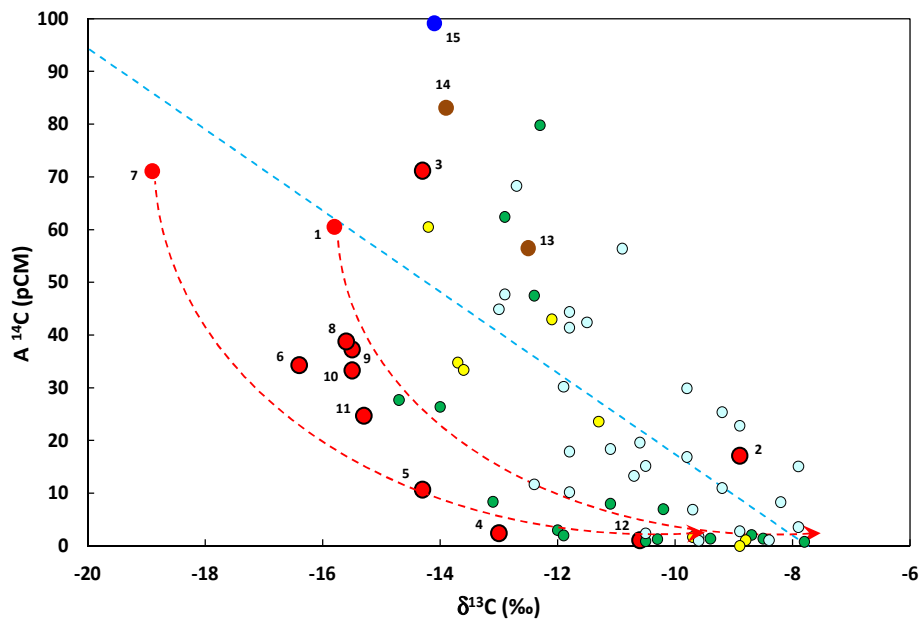
498

499 4.5.1. $\delta^{13}\text{C}$ and ^{14}C activities

500 Carbon isotopic compositions and ^{14}C activities, together with calculated ages are reported in
501 Table 4. Poussay, Mirecourt and Norroy waters (samples 4, 5 and 12) display the lowest
502 activities, which correspond to the oldest residence times. They also have the highest $\delta^{13}\text{C}$
503 values, together with the Saint-Genest groundwater (2) located apart from the Vittel-
504 Contrexéville area (Fig. 10).

505 ^{14}C activities have been corrected to account for interaction processes with the matrix and the
506 soil. The correction models that are utilized are the most appropriate for LTS (Celle-Jeanton et
507 al., 2009; Tab. 4). Corrected calculated ages (Tab. 4), corresponding to the groundwater
508 residence times in their aquifer, establish at around 15 ky for Mirecourt (5) and 32 ky for Norroy
509 (12). Surprisingly, the Poussay groundwater (4), sampled close to Mirecourt (Fig. 2), displays a
510 ^{14}C age ranging from 26.5 ky to 27.7 ky depending on the correction model, this is to say much
511 closer to the age of Norroy rather to the age of Mirecourt.

512



513
 514 Figure 10 : ^{14}C activities as a function of carbon isotopic compositions. Red circles correspond to LTS
 515 waters, brown circles to Muschelkalk waters, and the the blue circle to the Dogger springwater. Waters
 516 from the confined part of the LTS aquifer are marked by a bold black outline. Data from Blavoux and Olive
 517 (1981) are reported as yellow circles (southern part of the aquifer) and as blue circles for the northern
 518 part. Data from Celle-Jeanton et al. (2009) are reported as green circles. The blue dashed straight line
 519 represents the correlation of Blavoux and Olive (1981). The two red curves emphasize the likely evolution
 520 of LTS waters (Celle-Jeanton et al, 2009; this study). See text for more explanations.

521
 522 In contrast, LTS waters located south of the BVF, as well as the Saint-Genest groundwater (2)
 523 have higher ^{14}C activities. Corrected ages belong to the Holocene, which indicates a
 524 groundwater recharge posterior to the last glaciation. LTS waters from the unconfined part of
 525 the aquifer have quite young to recent ages (Tab. 4). This is also the case for the Rechaincourt
 526 water (3) from the confined aquifer (Fig. 2), but the anthropic contamination that has been
 527 evidenced may provide a valuable explanation for such a residence time. Finally, the Dogger
 528 and the two Muschelkalk waters are recent or present-day waters, as indicated by the corrected
 529 ^{14}C ages (Tab. 4)

530 Blavoux and Olive (1981) have evidenced a linear correlation between ^{14}C activities and $\delta^{13}\text{C}$
531 (Fig. 10). They attributed this correlation to a loss of dissolved CO_2 . Our data do not support
532 their conclusion, and better agree with a ^{14}C radioactive decay concomitant to interaction
533 processes with the aquifer (red dashed curves on Figure 10). Such an explanation is conversely
534 in good agreement with the conclusions of Celle-Jeanton et al. (2009), in spite of the fact that
535 the groundwaters they worked on come from the northern part of the aquifer, away from our
536 study area. These authors call for incongruent dissolution reactions and/or mixing under closed
537 system conditions to explain the $\delta^{13}\text{C}$ of the most evolved waters (i.e.; with the lowest ^{14}C
538 activity). The three waters that plot away from the curves (Fig. 10) have been found to contain
539 ^3H (Celle-Jeanton et al., 2009). This demonstrates that these groundwaters are very recent or
540 have been contaminated by present-day waters, as it is also probably the case for the
541 groundwater from Rechaincourt (3) which contains significant quantities of nitrates (Tab. 2).

542

543 4.5.2. Flowing velocities

544 From corrected ^{14}C ages, flowing velocities of the LTS groundwaters may be estimated as a
545 function of the distance from the recharge area (Tab. 5). However, this would require to
546 consider the leakage effects (Muschelkalk) and the contamination by lower triassic brines, as
547 sampled waters are mixtures between these three end-members (Fig. 6 to Fig. 9).

548

549

550

551

552

Sample	Mean of ¹⁴ C ages (y)	Distance from Recharge area (km)	Non corrected flowing velocity (m/y)	Transit time vs. recharge area (y)	Corrected flowing velocity vs. recharge area (m/y)
2 Saint-Genest	7653	15	1.96	5803	2.58
4 Poussay Val d'Arol	26902	20	0.74	24792	0.81
5 Mirecourt	15370	20	1.30	13260	1.51
6 Valfroicourt	6818	14.6	2.14	4708	3.10
8 Vittel	5405	10.3	1.91	3295	3.13
9 Frênes	5681	11.8	2.08	3571	3.30
10 Suriauville	6618	10.6	1.60	4508	2.35
11 Bulgnéville	8999	16.7	1.86	6889	2.42
12 Norroy	31706	40	1.26	29596	1.35
1 Etival-Clairefontaine	1850				
7 Relanges	2110				

553

554 Table 5 : Estimated flowing velocities for waters from the LTS aquifer (except Etival-Clairefontaine-1 and
555 Relanges-7, which are considered as recharge waters). Calculations were done with Etival-Clairefontaine
556 water for Saint-Genest, and with Relanges for the other waters, in accordance with piezometric data
557 (Vaute et al., 2013). Mean ages correspond to the average of the 4 corrected ages (Tab. 4). The non-
558 corrected flowing velocities refer to the distance from the recharge area divided by the mean ages, and
559 the corrected velocities to the distance from the recharge area divided by the transit time (that is to say
560 taking into account the fact that recharge waters have ¹⁴C ages different from 0).

561

562 It has been estimated above that the contribution of the triassic brines is very low in terms of
563 water budget. As a consequence, it was neglected to calculate flowing velocities. Considering
564 the influence of overlying waters from the Muschelkalk aquifer, any input will result in a lowering
565 of the calculated residence time, as Muschelkalk waters display "ages" close to 0 (Tab. 5), and
566 consequently it will overestimate flowing velocity.

567

568

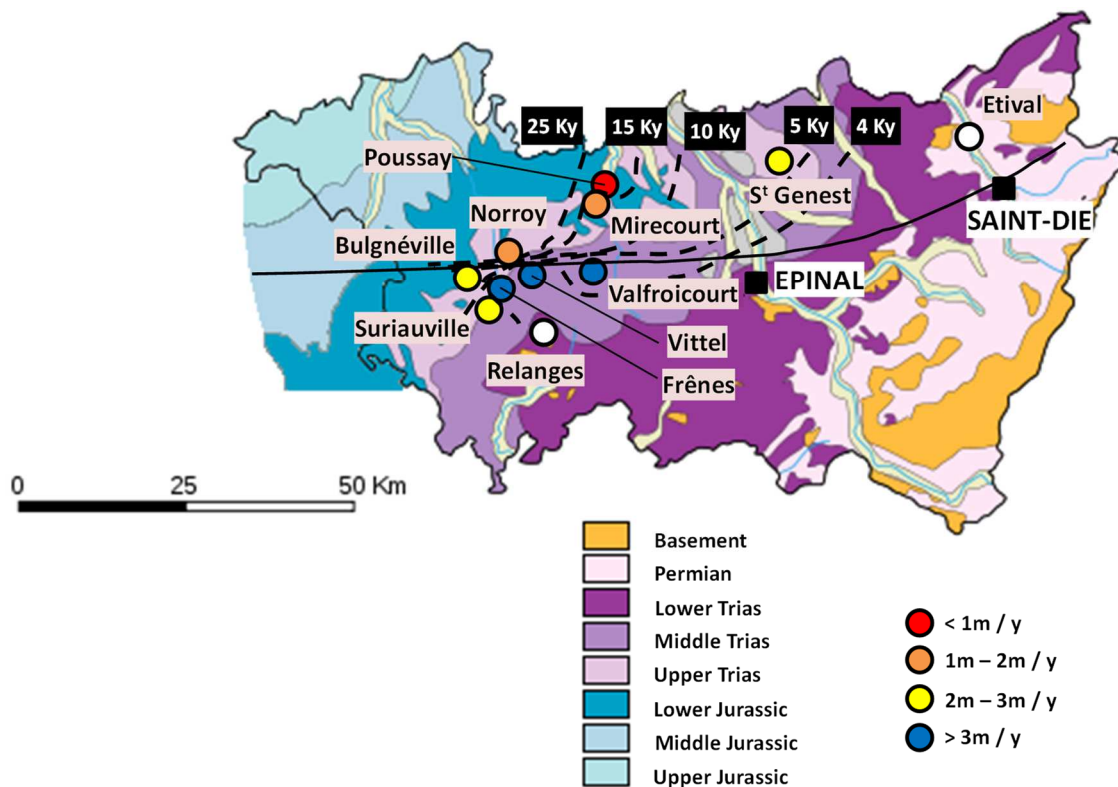
569

570

571

572

573



574

575 Figure 11 : ¹⁴C ages and flowing velocities for the LTS waters. The colours of the circles correspond to

576 the flowing velocities. Age curves have been tentatively drawn.

577

578 Figure 11 suggests that the distribution of flowing velocities is controlled by the BVF. The

579 highest velocities are found south of the fault. Corrected velocities are higher than 3 m/y for

580 waters 6 (Valfroicourt), 8 (Vittel) and 9 (Frênes). However, unlike Vittel and Frênes , there is no

581 evidence for an influence of Muschelkalk waters in the case of Valfroicourt (6), which thus

582 display the highest velocity of the study area, from 2 to 3 m/y whether flowing velocity is

583 corrected or not (Tab. 5). High velocities, in the range or higher than 2 m/y are also recorded for

584 waters from Saint-Genest (2), Suriauville (10) and Bulgnéville (11), although an overestimation

585 due to the influence of Muschelkalk waters likely occurs for Bulgnéville and is also possibly for

586 Suriauville (Fig. 9). Finally, waters north of the BVF (Poussay- Val d'Arol-4, Mirecourt-5, Norroy-

587 12) display lower velocities, even lower than 1 m/y for the Poussay-Val d'Arol water (4).

588 Such values are in good agreement with those of Blavoux and Olive (1981) (1.9 m/y) and are in
589 the range, though slightly lower, than the velocity given by Marty et al. (2003). It is also
590 remarkable to notice that for all the studied LTS waters, the flowing velocities decrease with
591 increasing distance from the recharge area (Fig. 11). This indicates that the velocity likely
592 decreases rapidly westwards, in agreement with very low velocities (0.05 m/y) that may be
593 derived from uranium activity ratios between the study area and the Meuse – Haute Marne site
594 (French radioactive waste storage area), located 60 km northwest (Innocent et al., 2015).

595

596 **5 - Conclusion**

597

598 The geochemical and isotopic study carried out on LTS groundwaters from the northeastern
599 Paris Basin demonstrates that they derive primarily from meteoric recharge waters. The isotopic
600 results depict the very slight influence of the lower triassic brines associated with the upper
601 Buntsandstein layers (*Voltzia* sandstones). In addition, some waters probably undergo the
602 contribution of groundwaters coming from the overlying Muschelkalk aquifer. This impact cannot
603 be further quantified however, as the corresponding geochemical end-member is insufficiently
604 constrained.

605 This study clearly points to the existence of leakage processes between the two aquifers, the
606 most important contribution of Muschelkalk waters occurring south of the BVF.

607 Residence times were calculated from ^{14}C data, allowing to estimate flowing velocities of LTS
608 groundwaters in the study area. They range from 1 to 3 m/y, approximately, and decrease
609 northwestwards. Waters north of the BVF display lower flowing rates, indicating (in addition to
610 leakage processes) that groundwater circulation in this area is constrained by the BVF.

611 Future work could aim at better constraining the influence of Muschelkalk waters. This would
612 clearly involve geochemical and isotopic studies on other Muschelkalk waters, in order to
613 precise as possible the characteristics of this end-member.

614

615 **Acknowledgements:** This research was co-funded by the Agence de l'Eau Rhin – Meuse
616 (AERM). We would like to thank M. Brach for his help in collecting samples. The work
617 benefited from the collaboration of BRGM laboratories for major, trace element and isotope
618 measurements.

619

620 **6. References**

621 **Aiuppa A., D'Alessandro W., Federico C., Palumbo B., Valenza M.** (2003) The aquatic
622 geochemistry of arsenic in volcanic groundwaters from Southern Italy. *Applied Geochemistry*
623 18, 1283–1296.

624 **Aiuppa A., Avino R., Brusca L., Caliro S., Chiodini G., D'Alessandro W., Favara R.,
625 Federico C., Ginevra W., Inguaggiato S., Longo M., Pecoraino G., Valenza M.** (2006)
626 Mineral control of arsenic content in thermal waters from volcano-hosted hydrothermal systems:
627 insights from island of Ischia and Phlegrean Fields (Campanian Volcanic Province, Italy).
628 *Chemical Geology* 229, 313–330.

629 **Berner R.A.** (1971) Worldwide sulfur pollution of rivers. *Journal of Geophysical Research* 76,
630 6597-6600.

631 **Blavoux B., Olive P.** (1981) Radiocarbon dating of groundwater of the aquifer confined in the
632 lower Triassic sandstones of the Lorraine region, France. *Journal of Hydrology* 54, 167-183.

633 **Celle-Jeanton H., Huneau F., Travi Y., Edmunds W.M.** (2009) Twenty years of groundwater
634 evolution in the Triassic sandstone aquifer of Lorraine: Impacts on baseline water quality.
635 *Applied Geochemistry* 24, 1198-1213.

636 **Claypool G.E., Holser W.T., Kaplan I.R., Sakai H., Zak I.** (1980) The age curves of sulfur and
637 oxygen isotopes in marine sulfate and their mutual interpretation. *Chemical Geology* 28, 199-
638 260.

639 **Craig H.** (1961) Isotopic variations in meteoritic waters. *Science* 133, 1702-1703.

640 **Eichinger L.** (1983) A contribution to the interpretation of ^{14}C groundwater ages considering the
641 example of a partially confined sandstone aquifer. In *Proceedings of the 11th International ^{14}C*
642 *Conference* (Stuiver M., Kra R.S. Eds.), *Radiocarbon* 25, 347-356.

643 **Evans G.V., Otlet R.L., Downing A., Monkhouse R.A., Rae G.** (1979) Some problems in the
644 interpretation of isotope measurements in United Kingdom aquifers. In *Isotope Hydrology II,*
645 *IAEA, Vienne*, 679-708.

646 **Fontes J.C., Garnier J.M.** (1979) Determination of the initial activity of the total dissolved
647 carbon. A review of the existing models and a new approach. *Water Resource Research* 12,
648 399-413.

649 **Fourniguet G.** (2012) Bilan sur les forages des gîtes hydrominéreaux A et B du secteur de
650 Contrexéville-Vittel (88) – Lorraine. Rapport BRGM/RP-61534-FR, 18 p., 4 ill., 3 ann.

651 **Fritz S.J., Drimmie R.J., Fritz P.** (1991) Characterizing shallow aquifers using tritium and ^{14}C :
652 periodic sampling based on tritium half-life. *Applied Geochemistry* 6, 17-33.

653 **Gély J.-P., Hanot F. et coll.** (2014) Le Bassin parisien. Un nouveau regard sur la géologie.
654 Cinquantenaire de l'Association des Géologues du Bassin de Paris, AGBP Ed., 230 p.

655 **Guendouz A., Michelot J.-L.** (2006) Chlorine-36 dating of deep groundwater from northern
656 Sahara. *Journal of Hydrology* 328, 572-580.

657 **Hogan J.F., Blum J.D.** (2003) Boron and lithium isotopes as groundwater tracers : a study at
658 the Fresh Kills Landfill, Staten Island, New York, USA. *Applied Geochemistry* 18, 615-627.

659 **Innocent C., Kloppmann W., Millot R., Vaute L.** (2015) U isotope systematics of groundwaters
660 from the Triassic aquifer of the northeastern Paris Basin and of the Rhine Graben, France.
661 *Procedia Earth and Planetary Sciences* 13, 112-115.

662 **Kloppmann W., Widory D., Pauwels H, Schomburgk S., Elsass P., Graveline N.** (2005)
663 Inventaire transfrontalier 2003 de la qualité des eaux souterraines de la vallée du Rhin
664 Supérieur. Etude isotopique (N, B) de l'origine des nitrates. Rapport BRGM/RP-54028-FR, 76 p.

665 **Marotel C., Minoux G.** (1973) Données géologiques et hydrogéologiques acquises à la date du
666 15.10.1973 sur la feuille topographique au 1/50.000 de Vittel (Vosges). Rapport BRGM/73-
667 SGN-322-NES, 28 p., 5 cartes.

668 **Marotel C., Minoux G.** (1975) Données géologiques et hydrogéologiques acquises à la date du
669 30 novembre 1975 sur la feuille topographique au 1/50.000 de Mirecourt (Meurthe-et-Moselle -
670 Vosges). Rapport BRGM/75-SGN-376-LOR, 36 p., 5 cartes.

671 **Matray J.-M., Meunier A., Thomas M., Fontes J.-C.** (1989) Les eaux de formation du Trias et
672 du Dogger du Bassin Parisien : histoire et effets diagénétiques sur les réservoirs. *Bulletin*
673 *Centre de Recherche d'Exploration et de Production Elf-Aquitaine* 13, 483-504.

674 **Marty B., Dewonck S., France-Lanord C.** (2003) Geochemical evidence for efficient aquifer
675 isolation over geological timeframes. *Nature* 425, 55-58.

676 **Mégrien C. et coll.** (1980) Synthèse géologique du Bassin de Paris. *Mémoires BRGM* 101,
677 102, 103.

678 **Meredith K., Moriguti T., Tomascak P., Hollins S., Nakamura E.** (2013) The lithium, boron
679 and strontium isotopic systematics of groundwaters from an arid aquifer system : Implications
680 for recharge and weathering processes. *Geochimica et Cosmochimica Acta* 112, 20-31.

681 **Millot R., Négrel P.** (2007) Multi-isotopic tracing ($\delta^7\text{Li}$, $\delta^{11}\text{B}$, $^{87}\text{Sr}/^{86}\text{Sr}$) and chemical
682 geothermometry : evidence from hydro-geothermal systems in France. *Chemical Geology* 244,
683 664-678.

684 **Millot R., Négrel P., Petelet-Giraud E.** (2007) Multi-isotopic (Li, B, Sr, Nd) approach for
685 geothermal reservoir characterization in the Limagne Basin (Massif Central, France). *Applied*
686 *Geochemistry* 22, 2307-2325.

687 **Millot R., Petelet-Giraud E., Guerrot C., Négrel P.** (2010a) Multi-isotopic composition ($\delta^7\text{Li}$,
688 $\delta^{11}\text{B}$, δD , $\delta^{18}\text{O}$) of rainwaters in France : Origin and spatio-temporal characterization. *Applied*
689 *Geochemistry* 25, 1510-1524.

690 **Millot R., Scaillet B., Sanjuan B.** (2010b) Lithium isotopes in island and geothermal systems :
691 Gaudeloupe, Martinique (French West Indies) and experimental approach. *Geochimica et*
692 *Cosmochimica Acta* 74, 1852-1871.

693 **Millot R., Innocent C., Blanc P., Guerrot C., Gaucher E., Négrel P.** (2011a) Apport de la
694 géochimie isotopique B-U-Li-Th appliquée aux eaux des formations de l'Oxfordien et du
695 Dogger. Rapport final. Rapport BRGM/RP-59480-FR, 57 p., 31 fig., 9 tabl., 1 ann.

696 **Millot R., Guerrot C., Innocent C., Négrel P., Sanjuan B.** (2011b) Chemical, multi-isotopic
697 (Li-B-Sr-U-H-O) and thermal characterization of Triassic formation waters from the Paris Basin.
698 *Chemical Geology* 283, 226-241.

699 **Minoux G.** (1966) Observations géologiques et hydrogéologiques complémentaires dans le
700 Bassin des eaux minérales de Vittel (Vosges), campagne de recherche 1964-65. Rapport
701 BRGM/66-SGR-A-042, 107 p., 1 ann.

702 **Minoux G.** (1967) Contribution à l'étude de la nappe aquifère de grès du Trias inférieur dans la
703 région de VITTEL – CONTREXEVILLE – LAMARCHE (Vosges). Inventaire et résultats des
704 campagnes de recherche 1954 – 1966. Suggestions pour la surveillance et le contrôle de la
705 réserve aquifère. Rapport BRGM/67-SGR-A-070, 30 p., 22 pht.

706 **Mook W.G.** (1980) Carbon-14 in hydrogeological studies. In P. Fritz and J.C. Fontes, eds,
707 Handbook of Environmental Isotope Geochemistry, vol. 1A, 49-74, Elsevier, Amsterdam, 545 p.

708 **Négrel P., Deschamps P.** (1996) Natural and Anthropogenic Budgets of a Small Watershed in
709 the Massif Central (France) : Chemical and Strontium Isotopic Characterization of Water and
710 Sediments. *Aquatic Geochemistry* 2, 1-27.

711 **Négrel P., Millot R., Brenot A., Bertin C.** (2010) Lithium isotopes as tracers of groundwater
712 circulation in a peat land. *Chemical Geology* 276, 119-127.

713 **Pearson F.J., Hanshaw B.B.** (1970) Sources of dissolved carbonate species in groundwater
714 and their effects on carbon-14 dating. In *Isotope Hydrology, IAEA, Vienne*, 271-286.

715 **Pennisi M., Gonfiantini R., Grassi S., Squarci P.** (2006) The utilization of boron and strontium
716 isotopes for the assessment of boron contamination of the Cecina River alluvial aquifer (central-
717 western Tuscany, Italy). *Applied Geochemistry* 21, 643-655.

718 **Rebeix R., Le Gal La Salle C., Michelot J.-L., Verdoux P., Noret A., Monvoisin G.,**
719 **Gianesinni S., Lancelot J., Simler R.** (2011) Tracing the origin of water and solute transfers in
720 deep groundwater from Oxfordian, Dogger and Trias formations in the east of the Paris Basin –
721 France. *Physics and Chemistry of the Earth* 36, 1496-1510.

722 **Rowland H.A.L., Omoregie E.O., Millot R., Jimenez C., Mertens J., Baciuc C., Hug S.J., Berg**
723 **M. (2011)** Geochemistry and arsenic behaviour in groundwater resources of the Pannonian
724 Basin (Hungary and Romania). *Applied Geochemistry* 26, 1-17.

725 **Teng F.Z., McDonough W.F., Rudnick R.L., Dalpé C., Tomascak P.B., Chappell B.W., Gao**
726 **S.** (2004) Lithium isotopic composition and concentration of the upper continental crust.
727 *Geochimica et Cosmochimica Acta*, 68, 4167-4178.

728 **Vaute L., Innocent C., Fourniguet G.** (2013) Actualisation du modèle hydrogéologique de la
729 nappe des grès du Trias en Lorraine. Rapport BRGM/RP-62405-FR, 56p., 20 fig., 4 tabl.

730 **Widory D., Petelet-Giraud E., Négrel P., Ladouche B.** (2005) Tracing nitrate sources in
731 groundwater by coupled nitrogen and boron isotopes : A synthesis essay. *Environmental*
732 *Science and Technology* 39, 2, 539-548.

733 **Wigley T.M.L.** (1975) Carbon-14 dating of groundwater from closed and open systems. *Water*
734 *Resource Research* 11, 324-328.

735 **Wigley T.M.L.** (1976) Effect of mineral precipitation on isotopic composition and ¹⁴C dating of
736 groundwater. *Nature* 263, 219-220.